NASA TECHNICAL NOTE

NASA TN D-5410

THE DYNAMIC RESPONSE OF A FLEXIBLE ROTOR BLADE TO A CONCENTRATED FORCE MOVING FROM TIP TO ROOT

by John F. Ward

Langley Research Center

Langley Station, Hampton, Va.

NATIONAL AERONAUTICS AND SPACE ADMINISTRATION • WASHINGTON, D. C. • SEPTEMBER 1969

1. Report No. NASA TN D-5410	2. Government Accession No.	3. Recipient's Catalog No.
4. Title and Subtitle THE DYNAMIC RESPONSE OF A FLEXIBLE ROTOR BLADE TO A CONCENTRATED FORCE MOVING FROM TIP TO ROOT		5. Report Date September 1969 6. Performing Organization Code
7. Author(s) John F. Ward		8. Performing Organization Report No. L-6381
9. Performing Organization Name and Address NASA Langley Research Center Hampton, Va. 23365		10. Work Unit No. 721-02-10-05-23 11. Contract or Grant No.
12. Sponsoring Agency Name and Address National Aeronautics and Space Administration Washington, D.C. 20546		13. Type of Report and Period Covered Technical Note 14. Sponsoring Agency Code

15. Supplementary Notes

Material herein was presented, in part, in AIAA Paper No. 69-203, "The Dynamic Response of a Flexible Rotor Blade to a Tip-Vortex Induced Moving Force," by John F. Ward and William J. Snyder, Feb. 1969.

16. Abstract

An approximate analytical solution is presented of the dynamic response of a flexible rotor blade to a radially moving force. The results are interpreted specifically in terms of helicopter rotor-blade vibration characteristics associated with tip-vortex impingement. These results indicate that low-frequency-mode resonant amplification of repetitive-impulse loadings may be encountered at moderate to high forward speeds on lifting rotor systems. The resonant conditions are encountered in sequence with increasing forward speed. For blades of conventional design, the resonant frequencies are encountered at noninteger multiples of rotor rotational speed.

17. Key Words Suggested by Author(s) Flexible rotor blade Moving force Blade bending moments	18. Distribution Statement Unclassified – Unlimited

19. Security Classif. (of this report) Unclassified	20. Security Classif. (of this page) Unclassified	21. No. of Pages 41	22. Price* $3.00

*For sale by the Clearinghouse for Federal Scientific and Technical Information Springfield, Virginia 22151

THE DYNAMIC RESPONSE OF A FLEXIBLE ROTOR BLADE TO A CONCENTRATED FORCE MOVING FROM TIP TO ROOT*

By John F. Ward
Langley Research Center

SUMMARY

An analysis is presented for an approximate solution of the dynamic response of a flexible rotor blade to a radially moving force. The results are interpreted specifically in terms of helicopter rotor-blade vibration characteristics associated with tip-vortex impingement. These results indicate that low-frequency-mode resonant amplification of repetitive-impulse loadings may be encountered at moderate to high tip-speed ratios on lifting rotor systems. The mode-resonance conditions are encountered in sequence with increasing tip-speed ratio. The blade natural modes can be forced in resonance at the design natural frequencies, which are usually placed at noninteger multiples of rotor rotational speed to minimize blade response to harmonic air loads. The results of the present analysis suggest that additional attention may have to be given to the selection of blade design natural frequencies in order to minimize the response to a repetitive-impulse moving force.

INTRODUCTION

The impingement of tip vortices, trailing from helicopter rotor blades upon following blades, has been identified as a source of dynamic air loads, vibration, noise, and oscillating stress. This vortex-blade interaction, illustrated in figure 1, has been treated in a number of investigations including references 1 to 10. A unique aspect of this type of dynamic loading is the radial movement of the trailing vortex along the following blade. The pattern of movement on the following blade is systematic and is basically determined by the number of blades in the rotor and the rotor tip-speed ratio μ, which is defined as the ratio of the forward velocity V_f to the product of the rotor speed Ω and tip radius R.

Emphasis in the past has been on the configurations of low tip-speed ratio ($\mu < 0.25$), where the trailing vortex movement is restricted to the outer portions of the following

*Material herein was presented, in part, in AIAA Paper No. 69-203, "The Dynamic Response of a Flexible Rotor Blade to a Tip-Vortex Induced Moving Force," by John F. Ward and William J. Snyder, Feb. 1969.

blade. It is becoming increasingly evident that the problem may be of concern throughout the operational envelope for both "pure" and "compound" helicopter lifting rotor systems, as indicated in references 11, 12, and 13. At moderate to high tip-speed ratios ($\mu > 0.25$), there is a basic change in the nature of the movement of the trailing tip vortex relative to the following blade. The vortex movement is no longer restricted to the outer portion of the following blade. The point of vortex-blade intersection therefore moves completely across the full length of the blade from tip to root at very high relative velocities. This full sweep of the blade by a moving loading is the primary reason for concern. As noted in reference 14, when a loading moves along a beam at unique critical speeds, resonant situations exist which induce increased beam vibrations.

The objective of the present paper is to provide some insight into the dynamic response characteristics specifically associated with the high-velocity radial movement of an isolated loading along the blade. The present analysis identifies some of the resonant conditions which may exist within the operating envelope of pure and compound helicopter lifting rotor systems. A basic premise of the present analysis is the presence of a strong trailing vortex in close vertical proximity to a following blade. It is acknowledged that this condition may not exist for certain operating conditions such as zero rotor lift on compound helicopters or cases where combinations of rotor lift and propulsive force produce rapid movement of the trailing wake away from the rotor tip-path plane.

This analysis does not treat a fundamentally new dynamic problem, since there are existing generalized aeroelastic rotor computer programs which include, within detailed aerodynamic and dynamic subprograms, all the ingredients of concern in the present analysis. Therefore, this simple analysis merely isolates a particular aspect of rotor dynamics and emphasizes the blade response to radially moving forces in hopes of gaining some additional insight.

The loading used in this initial analysis is a concentrated unit force. The prediction of the actual vortex-induced loading on a following blade depends upon an accurate definition of the free wake of the lifting rotor. The detailed consideration of typical vortex-induced blade loadings, such as moment couples or locally distributed loadings, are not specifically treated in the present analysis. The moving-force analysis is considered to be a reasonable first step for the purpose of illustrating basic trends in blade-response characteristics, such as resonant conditions, single-impulse response as compared with repetitive-impulse response, and associated blade-root bending-moment time histories. The analysis illustrates cantilever-blade-response characteristics, and the implications of the results are treated in relation to helicopter rotor vibration. The derivation of the equations of motion is presented in the appendix.

SYMBOLS

a_i	frequency parameter related to velocity of moving force, $\left(\frac{k_i R}{R}\right)v$, radians per second
C(x)	damping coefficient at point x on blade, $\frac{\text{lbf}}{\text{ft/sec}}$ $\left(\frac{\text{newtons}}{\text{meter/sec}}\right)$
d	distance from free end of blade to point of load application, ft (meters)
EI	blade bending stiffness, lbf-ft^2 $\left(\text{newton-meters}^2\right)$
F(x,t)	time-varying force applied to blade, lbf (newtons)
$F_d(x,t)$	time-varying damping force applied to blade, $\frac{\text{lbf}}{\text{ft/sec}}$ $\left(\frac{\text{newtons}}{\text{meter/sec}}\right)$
g	gravitational acceleration constant, ft/sec^2 $\left(\text{meters/sec}^2\right)$
K_i	rotating-blade Southwell coefficient
k_i	normal-mode coefficient
$k_i R$	eigenvalues of frequency equation for simple, uniform, nonrotating blade
$M(x,t_1)$	time-varying blade bending moment at point x, lbf-ft (newton-meters)
m	mass per unit length of blade, $\frac{\text{slugs}}{\text{ft}}$ $\left(\frac{\text{kilograms}}{\text{meter}}\right)$
M_w	blade deadweight moment at fixed end, $\frac{mgR^2}{2}$, lbf-ft (newton-meters)
n	total number of modes considered
P(t)	time-varying magnitude of concentrated load on blade, lbf (newtons)
q(t)	time-varying magnitude of nondimensional concentrated load on blade
q_o	nondimensional unit force, where applied force P(0) at t = 0 is equal in magnitude to blade weight mRg
R	blade radius, ft (meters)

t	time, sec
t_1	instant of time for which blade dynamic response is calculated, sec
$V(x,t_1)$	time-varying shear force at point x on blade, lbf (newtons)
V_f	forward velocity of aircraft, ft/sec (meters/sec)
v	relative velocity of radially moving force, measured along blade span, positive when moving from tip to root, ft/sec (meters/sec)
$X_i(x), X_j(x)$	modal displacement of ith and jth mode, respectively, at point x on blade
x	radial coordinate along blade, measured from free end, ft (meters)
y	blade lateral displacement, ft (meters)
α_i	coefficient used in characteristic modal functions
$\delta(x - d)$	Dirac delta function
ϵ	nondimensional rate of change of magnitude of applied concentrated unit force, $\frac{\Delta q(t)/\Delta t}{q_o/\tau}$
μ	rotor tip-speed ratio, $V_f/\Omega R$
ν_i	assigned value of modal damping coefficient
τ	time interval during which force is on blade, sec
$\varphi(t)$	time-varying mode participation factor, ft (meters)
ψ	blade azimuth angle measured from downwind position in direction of rotation, deg
$\Delta\psi$	azimuth increment corresponding to time of vortex movement along blade, deg
Ω	rotor rotational speed, radians/sec

ω blade bending natural frequency, radians/sec

$\theta(x,t_1)$ time-varying slope of blade deflection curve at point x, radians

A_i, B_i, $\overline{B}_i$, E_i, $\overline{E}_i$ frequency parameters defined in equations (A38) of appendix

$C_{i,\epsilon,1},\ldots,C_{i,\epsilon,4}$, $\overline{C}_{i,\epsilon,1},\ldots,\overline{C}_{i,\epsilon,4}$ coefficients in equations (A34) and (A35) of appendix for ith-mode participation factors; these coefficients are defined in equation (A37) and are related to an applied force with a linear variation in magnitude with time ($\epsilon \neq 0$)

$C_{i,0,1},\ldots,C_{i,0,4}$, $\overline{C}_{i,0,1},\ldots,\overline{C}_{i,0,4}$ coefficients in equations (A34) and (A35) of appendix for ith-mode participation factors; these coefficients are defined in equation (A36) and are associated with an applied force of constant magnitude ($\epsilon = 0$)

Subscripts:

C chordwise degree of freedom, blade motions in plane of rotor rotation

d damped

F flapwise degree of freedom, blade motions perpendicular to plane of rotor rotation

i,j mode number

R rotating

A prime indicates a derivative with respect to x.

A dot indicates a derivative with respect to time.

TIP-VORTEX MOVEMENT

The basic concern in the present analysis is the radial movement of the trailing vortex from the leading blade of a helicopter along the following blade. The path of a tip vortex deposited into the rotor wake by a given blade will describe a systematic helical pattern when viewed from above the rotor disk. The instantaneous point of the intersection of the following blade and the trailing tip-vortex helix (point A in fig. 1) depends upon rotor tip-speed ratio μ and the number of blades.

An example of the resulting radial movement of the point of blade-vortex intersection along the following blade for a three-blade rotor is shown in figure 2. This figure, similar to figures presented in reference 1, illustrates typical variations of the intersection point as a function of azimuth position ψ of the following blade for a range of tip-speed ratios from 0.2 to 1.0. The point A on the $\mu = 0.2$ line in figure 2 corresponds to the same point in the illustrated example shown in figure 1. The effects of wake contraction, neglected in this presentation, will cause slight changes in detail but will not alter the basic pattern variation with increasing tip-speed ratio. At tip-speed ratios below approximately 0.25, the tip-vortex path moves onto the following blade at an azimuth angle ψ of about 80°, moves inboard on the blade, and then returns to the tip. As the tip-speed ratio is increased above 0.25, a basic change occurs in the pattern of movement. The point of intersection again starts at the tip but continues to move inboard along the entire blade until it leaves the blade at the root end, instead of returning to the tip. Further increase in tip-speed ratio results in increasing the relative velocity of the movement of the point of intersection along the blade.

The situation will change somewhat with the number of blades in a given rotor, as shown in figure 3. An increase in the number of blades decreases the interval between the leading and the following blade. This decrease, in turn, increases the tip-speed ratio at which the vortex path changes from leaving the blade at the tip to leaving the blade at the root.

The vortex-blade intersection patterns for a three-bladed rotor shown in figure 2 result in the range of radial velocities of vortex movement presented in figure 4. This figure presents the variation in the average velocity of radial movement of the vortex-blade intersection point along the following blade. Figure 4 is based upon an assumed operating tip speed ΩR of 650 feet per second (198 meters per second). The curve begins at $\mu = 0.25$, which corresponds to the tip-speed ratio at which the vortex begins to sweep over the entire blade and moves off the following blade at the root end. Typical relative velocities are 250 to 600 feet per second (76 to 182 meters per second) for a range of tip-speed ratio from 0.25 to 1.0.

ANALYTICAL METHOD USED IN DETERMINING BLADE DYNAMIC RESPONSE

The dynamic response which is amenable to analytical solution applies to the force moving along the following blade at constant velocity. This situation is approached as the tip-speed ratio increases above 0.25. For tip-speed ratios below 0.25, the intersection point of the tip-vortex path and the blade moves along the blade with a varying velocity and results in blade-response equations of motion with time-varying coefficients. Some insight into these low tip-speed-ratio responses may be gained from the constant velocity solutions, but the practical determination of the varying velocity responses requires the utilization of numerical integration techniques.

The problem of determining the dynamic response of a flexible rotor blade to a moving force is analogous to the problem of a concentrated load moving across a simple beam, which has been treated by a number of investigators (refs. 14, 15, and 16). The principal concern in the past has been with severe vibration induced in bridge structures by vehicles moving at critical speeds. The analytical method developed herein treats the adaptation of the simple beam analysis of reference 14 to a rotating cantilever beam and the interpretation of the results in terms of conventional helicopter-rotor-system parameters. The analysis is readily adaptable to hinged rotor blades with the proper substitution of hinged blade-mode shapes, frequencies, and damping coefficients in place of those of the cantilever blade.

Assumptions

The basic assumptions, which result in an approximation of the rotating rotor blade dynamic response characteristics, are as follows:

(1) The rotor blade has uniform mass and stiffness distribution.

(2) The mode shapes of the rotating flexible blade are reasonably approximated by the uncoupled mode shapes for a nonrotating uniform beam.

(3) The analysis, developed for the flapwise degree of freedom, can also be applied to the chordwise degree of freedom by assigning appropriate values of the rotating-blade natural frequencies and damping coefficients.

(4) The periodic variations in aerodynamic damping caused by increasing forward speed are neglected.

(5) The vortex-induced blade loading is considered to be sufficiently localized in relation to the blade radius so that it may be treated as a point load of constant or linearly varying magnitude, moving at constant velocity along the blade. (This concept is acknowledged to be an oversimplification of the real situation in light of such factors as vertical

displacement of the vortex in the nonrigid wake, time variations in blade lift, vortex decay, and complex blade-wake interaction.)

(6) Only the tip-vortex trailing from a single leading blade is considered.

(7) The analysis is performed on the basis of an arbitrary "unit force" which is nondimensionalized by the weight of the blade.

Equations of Motion

The equations giving the undamped and damped, forced and free response for the cantilever blade arrangement shown in figure 5 are developed in the appendix. In the analysis the force is assumed to move from the blade tip to the blade root at a constant velocity v and the nondimensional unit force is assumed to vary as a linear function of time. The manner in which this unit force $q(t)$ varies with time is illustrated in figure 6. The time interval τ, indicated in figure 6, represents the time it takes the force to move the length of the blade R at constant velocity v.

Sample Applications

A few sample applications are presented and discussed in the following section to illustrate the type of blade response that might result from tip-vortex impingement at moderate to high tip-speed ratios. The approximate analysis is applied to both the flapwise and chordwise degrees of freedom by using the respective rotating natural frequencies and assuming that the nonrotating normal mode shapes adequately approximate the rotating mode shapes in all examples. The basic characteristics for the cantilever blade used in the sample cases are listed in table 1.

RESULTS AND DISCUSSION

Resonant Conditions

Just as is true for the stationary simple beam, the rotating blade experiences resonant response characteristics when specific values of the frequency parameter a_i in equation (A39) of the appendix become equal to a given mode natural frequency ω_{iR}. Since a_i is a function of the velocity of the moving force and, in turn, of tip-speed ratio, resonant conditions will be encountered at specific tip-speed ratios.

The relative velocity v at which resonant conditions exist is determined as follows:

At resonance

$$a_i = \omega_{iR}$$

and equation (A28) gives

$$a_i = \left(\frac{k_i R}{R}\right) v$$

Therefore,

$$v = \omega_{iR}\left(\frac{k_i R}{R}\right)^{-1}$$

With the relative velocities determined in this manner, the critical tip-speed ratios can be obtained from figure 4 for a three-blade rotor with a tip speed ΩR of 650 feet per second (198 meters per second).

Applying this approach to the sample cantilever blade described in the previous section results in the critical tip-speed ratios shown in figure 7. Resonant conditions, implying increased rotor vibration, are encountered in the flapwise modes (indicated in fig. 7 by the circular symbols) at a tip-speed ratio of approximately 0.5. The first three flapwise bending modes are encountered almost simultaneously, and the fourth and higher modes are encountered in sequence at higher tip-speed ratios. Applying the same approach to the chordwise bending degree of freedom results in a predicted resonance for the first mode at a tip-speed ratio in the vicinity of 0.7 (shown by the square symbol in fig. 7). This example indicates the general trend in resonant points. The points shift somewhat with changes in blade frequencies, tip speed, and number of blades. For example, most of the hinged-blade mode resonant responses are encountered over the same range of tip-speed ratios as shown in figure 7. However, the hinged-blade chordwise rigid-body mode, with the natural frequency a subharmonic of rotor rotational speed, can have a critical tip-speed ratio as low as 0.3.

A decrease in the number of blades at a given tip-speed ratio increases the radial velocity of the tip vortex induced moving force. This trend can be observed in figure 3 by noting the increase in the slope of the vortex-movement curves with decreasing number of blades for a constant tip-speed ratio $\mu = 1.0$. This result means that a given resonant radial velocity will be achieved at a lower tip-speed ratio when the number of blades is decreased. Conversely, the addition of blades can decrease the radial velocities and delay resonance to higher tip-speed ratios.

The moving force is on the blade during only a portion of each rotor revolution. Therefore, the resonant blade motion will not expand continuously as a function of time. While the moving force is on the blade, during the time interval τ, the equation for the forced response mode participation factor at resonance is as follows:

For $a_i = \omega_{iR}$, $0 < t_1 < \tau$, $\nu_i = 0$, and $\epsilon = 0$,

$$\varphi_{iR}(t_1) \approx \frac{q_0 g}{2\alpha_i^2 \omega_{iR}^2}\Big[\sinh \omega_{iR} t_1 + \alpha_i(\cosh \omega_{iR} t_1 - \cos \omega_{iR} t_1) - t_1 \omega_{iR}(\cos \omega_{iR} t_1 - \alpha_i \sin \omega_{iR} t_1)\Big]$$

This equation was derived from equation (A39), which is given in the appendix. Since equation (A39) is indeterminate at resonance, $a_i = \omega_{iR}$, this equation was obtained by taking the

$$\lim_{a_i \to \omega_{iR}} \left[\frac{f'(a_i)}{F'(a_i)}\right]$$

where $f'(a_i)$ and $F'(a_i)$ are the derivatives of the numerator and denominator, respectively, of equation (A39).

Blade-Root Bending Moments

The following examples and discussion deal with the basic cantilever blade described in table 1. Examples of single- and repetitive-impulse blade-root bending-moment response are given. Both the flapwise and chordwise degrees of freedom are discussed as required for illustrative purposes. The damping used in various cases is assigned to cover a range of values considered to be representative of cantilever blade designs. These constant damping coefficients are assumed to include both structural and aerodynamic damping. The periodically varying damping coefficients which result from the effects of increasing tip-speed ratio cannot be treated in this approximate analysis.

The specific examples considered in the following discussion are listed in table 2. The fourth flapwise bending mode, identified in figure 7, is not included in these sample cases.

Single impulse.- If the damping is sufficient to reduce the response to insignificant levels within one rotor revolution, a single-impulse analysis can be used. This type of analysis generally applies in the flapwise degree of freedom where aerodynamic damping is significant. Examples of the blade-root flapwise-bending-moment variation with time for a single-impulse loading are shown in figure 8, which presents three examples of the damped response to the impingement of a moving unit force. These three examples represent situations where the concentrated force is moving along the blade at relative velocities of 248 feet per second (75 meters per second) when $\Delta\psi = 150^\circ$, 372 feet per second (113 meters per second) when $\Delta\psi = 100^\circ$, and 466 feet per second (142 meters per second) when $\Delta\psi = 80^\circ$. These results are considered to be analogous to tip vortices encountered at tip-speed ratios of approximately 0.3, 0.5, and 0.7, respectively.

The single-impulse results shown in figure 9 are for a tip-speed ratio of 0.7 with reduced modal damping. The transient response persists for more than 2 revolutions and the difference between the two response signatures is the result of using a moving force of constant magnitude in one case ($\epsilon = 0$), shown by the solid line, and a moving force decreasing linearly to zero ($\epsilon = -1$) in time τ, shown by the dashed line.

Repetitive impulse.- The rotating blade experiences a tip-vortex-induced impulse loading each revolution. If the combined aerodynamic and structural damping is low, the free vibration will persist over a number of rotor revolutions. This response may be approximated by the superposition of a series of single-impulse response time histories. The summation is continued for a sufficient number of rotor revolutions to achieve steady-state conditions. An example of low damping can be considered in either the flapwise or chordwise degree of freedom.

Chordwise degree of freedom: The chordwise case is considered here first for illustrative purposes. The example shown in figure 10 represents a typical blade-root chordwise-bending-moment time history at a tip-speed ratio of approximately 0.3. The low level of damping assigned to this response is assumed to represent a typical chordwise-mode damping which consists of structural damping and little or no aerodynamic damping. The second and higher chordwise modes are not considered because of the wide frequency separation between the fundamental and second chordwise modes.

The solid curve in figure 10 represents the blade-root chordwise-bending-moment response to the initial impulse in the first rotor revolution. Because of the low damping, the transient response persists over many revolutions. Eventually, the repetitive-impulse response will stabilize on a steady-state response represented by the dashed curve in figure 10. This steady-state response, after 10 rotor revolutions, appears as a distorted once-per-rotor revolution periodic oscillation.

Increasing the tip-speed ratio for the example shown in figure 10 from 0.3 to 0.7 results in the root-bending-moment signatures shown in figure 11. Here again the chordwise-moment time history is shown for the initial revolution and the steady-state case in the tenth revolution. The result shown in figure 11 has a peak-to-peak response which is lower than the response for a tip-speed ratio of 0.3 in figure 10. This result is true even though the result at a tip-speed ratio of 0.7 is close to a critical tip-speed ratio for the chordwise mode indicated in figure 7. This decrease in response results from a specific combination of forced and transient response of the blade when rotated at a non-integer multiple of the chordwise fundamental bending-mode natural frequency (in this case $\Omega/\omega_{iR} = 0.7$). In addition, the time interval τ during which the force is on the blade decreases with increasing tip-speed ratio.

Flapwise degree of freedom: An example of the type of response that might be encountered in the flapwise degree of freedom, with low damping in each mode, is shown

in figure 12. Both the single-impulse and repetitive-impulse signatures are shown. The repetitive-impulse loading again results in a steady-state signature (repeating every rotor revolution) that is a mixture of the forced and transient response of the blade flapwise modes. This combination gives a rather complex response, which would prove difficult to interpret realistically on the basis of applying conventional harmonic analysis techniques.

Further Comments

Generalizations, similar to those for a simple harmonic forced response, are difficult to state for the repetitive impulse response. Calculated time histories of blade response for a wide range of conditions suggest that the maximum response for conventional blade designs will occur in the tip-speed-ratio range from 0.25 to 0.35. The analytical results also confirm that, as expected, when the blade natural frequencies are placed at integer multiples of rotor rotational speed, and the low frequency modes are lightly damped, the response to repetitive-impulse loading can build to very large amplitude.

Proper tuning of the rotor-blade frequencies to specific noninteger multiples of rotor rotational speed may make it possible to attenuate the blade response to tip-vortex repetitive-impulse loadings. This situation suggests the need for some additional attention in the selection of design natural frequencies of the blade to avoid the amplification of harmonic airloads. In this connection, reference 17 treats some of the fundamental aspects of tuning dynamic systems to achieve minimum response to repetitive impulse. Also, reference 18 treats a case of helicopter rotor dynamic stability associated with response to repetitive impulse.

The examples presented in this paper are for a cantilever, or hingeless, rotor blade. The method may be applied to hinged blades as well. The resulting critical tip-speed ratios will be similar to those of the cantilever blade and will be directly related to the particular natural frequencies, tip speed, and number of blades of the hinged rotor system.

A further extension in the analysis would utilize rotating mode shapes in order to provide increased accuracy in the response calculations. Each rotating mode may be included in the analysis as an expansion in normal modes of a nonrotating blade. The expansion method is discussed in reference 19. Some insight into the case of nonconstant velocity of the moving force, which applies to low tip-speed-ratio ($\mu < 0.25$) conditions, can be obtained by considering classical dynamic response during an acceleration or deceleration through critical shaft speeds, as discussed in references 16 and 20.

CONCLUDING REMARKS

An analytical study of rotor-blade dynamic response to impulse loading indicates that low-frequency-mode resonant amplification can be induced by the force moving at high velocity from the tip to the root of the blade. The practical implication of this phenomenon is that the situation is analogous in many respects to the impingement of a trailing tip vortex upon following rotor blades at moderate and high forward speeds. Interpreting the results in relation to tip-vortex movement along a rotor blade indicates that blade mode resonance may be encountered at specific tip-speed ratios. These mode resonant points are characterized by increased blade vibration and are encountered in sequence at increasing tip-speed ratios above a value of approximately 0.25. The blade natural modes can be forced in resonance at the design natural frequencies, which are usually placed at noninteger multiples of rotor rotational speed to minimize response to harmonic air loads. The results of the present analysis suggest the need for additional attention in the selection of blade design natural frequencies in order to minimize the response to a repetitive-impulse moving force.

Langley Research Center,
National Aeronautics and Space Administration,
Langley Station, Hampton, Va., May 15, 1969,
721-02-10-05-23.

APPENDIX

EQUATIONS OF MOTION

The cantilever-beam arrangement shown in figure 5 rotates at constant angular velocity Ω. The x,y-coordinate system rotates with the beam with the origin at the point of the undeflected, free end of the cantilever beam. This selection of an unconventional coordinate system resulted from the primary concern for studying beam response for loadings moving onto the beam at the free end ($x = 0$) at the initial time ($t = 0$) and moving radially at constant velocity v to the fixed end of the beam at $x = R$ and $t = \tau$.

The analysis proceeds by first developing the equations of motion for a nonrotating beam, $\Omega = 0$, by the methods of reference 14, and then using these results to provide an approximate analysis for a rotating blade. The approximation is achieved by assuming that mode shapes for a nonrotating beam adequately represent the mode shapes for a rotating blade and that the natural frequencies of the rotating blade can be calculated by accounting for centrifugal stiffening effects by the method of reference 17.

Nonrotating Beam

The governing differential equation of forced motion of the nonrotating beam is

$$m\ddot{y}(x,t) + \left[EIy''(x,t)\right]'' = F(x,t) \tag{A1}$$

The external forces acting on the beam are the viscous damping force and a concentrated force P at a point $x = d$:

$$F(x,t) = F_d(x,t) + P_{x=d}(t) \tag{A2}$$

where the viscous damping force is a function of local beam velocity

$$F_d(x,t) = -C(x)\dot{y}(x,t) \tag{A3}$$

where $C(x)$ is the local damping coefficient at point x. Therefore, equation (A1) becomes

$$m\ddot{y}(x,t) + C(x)\dot{y}(x,t) + \left[EIy''(x,t)\right]'' = P_{x=d}(t) \tag{A4}$$

Using the Galerkin method permits the deflection $y(x,t)$ to be represented by a superposition of modal deflection functions as follows:

APPENDIX

$$y(x,t) = \sum_{j=1}^{n} \varphi_j(t) X_j(x) \tag{A5}$$

where the functions $X_j(x)$ are the normal mode shapes satisfying the equation

$$\left[EIX_j''(x)\right]'' - m\omega_j^2 X_j(x) \equiv 0 \tag{A6}$$

The functions $\varphi_j(t)$ are the mode participation factors and ω_j is the frequency of oscillation of the jth mode.

Substituting equation (A5) into equation (A4) gives

$$\sum_{j=1}^{n} \left\{ \varphi_j(t) \left[EIX_j''(x)\right]'' + mX_j(x)\ddot{\varphi}_j(t) + C(x)\dot{\varphi}_j(t)X_j(x) \right\} = P_{x=d}(t) \tag{A7}$$

Applying equation (A6) to equation (A7) gives

$$\sum_{j=1}^{n} \left[m\ddot{\varphi}_j(t) + C(x)\dot{\varphi}_j(t) + m\omega_j^2 \varphi_j(t) \right] X_j(x) = P_{x=d}(t) \tag{A8}$$

Multiplying equation (A8) by $X_i(x)$ and integrating over the length of the beam, the orthogonality of the modal functions

$$\int_0^R X_i(x)X_j(x)\,dx = 0 \qquad (i \neq j) \tag{A9}$$

permits equation (A9) to be simplified to

$$m\ddot{\varphi}_i(t) \int_0^R X_i^2(x)\,dx + \sum_{i=1}^{n} \dot{\varphi}_i(t) \int_0^R C(x)X_i(x)X_j(x)\,dx + m\omega_i^2 \varphi_i(t) \int_0^R X_i^2(x)\,dx$$

$$= \int_0^R P_{x=d}(t)X_i(x)\,dx \tag{A10}$$

Neglecting the intermodal coupling due to damping gives i uncoupled differential equations for the mode participation factors:

APPENDIX

$$\ddot{\varphi}_i(t) + \frac{\int_0^R C(x)X_i^2(x)\,dx}{m\int_0^R X_i^2(x)\,dx}\,\dot{\varphi}_i(t) + \omega_i^2\varphi_i(t) = \frac{\int_0^R P_{x=d}(t)X_i(x)\,dx}{m\int_0^R X_i^2(x)\,dx} \tag{A11}$$

The term $\int_0^R P_{x=d}(t)X_i(x)\,dx$ can be represented by $\int_0^R P(t)\delta(x-d)X_i(x)\,dx$ where the function $\delta(x-d)$ is the Dirac delta function and

$$\int_0^R P(t)\delta(x-d)X_i(x)\,dx = P(t)X_i(d)$$

Equation (A11) becomes

$$\ddot{\varphi}_i(t) + \frac{\int_0^R C(x)X_i^2(x)\,dx}{m\int_0^R X_i^2(x)\,dx}\,\dot{\varphi}_i(t) + \omega_i^2\varphi_i(t) = \frac{P(t)X_i(d)}{m\int_0^R X_i^2(x)\,dx} \tag{A12}$$

The normal functions and frequency equation for a free-clamped beam are developed as follows:

The general solution for the free lateral vibration of a simple uniform beam is of the form

$$X_i = C_1 \sin k_i x + C_2 \cos k_i x + C_3 \sinh k_i x + C_4 \cosh k_i x \tag{A13}$$

For the cantilever beam of figure 5, the following boundary conditions apply:

Clamped end, $x = R$:

Deflection	$X_i = 0$
Slope	$\frac{dX_i}{dx} = 0$

Free end, $x = 0$:

Moment	$\frac{d^2X_i}{dx^2} = 0$
Shear	$\frac{d^3X_i}{dx^3} = 0$

Applying these boundary conditions to equation (A13) and its derivatives and setting the resulting determinant equal to zero gives the following frequency equation:

$$\cos k_i R \cosh k_i R = -1 \tag{A14}$$

This frequency equation has an infinite set of solutions, the first four of which are:

$$k_1 R = 1.876$$

$$k_2 R = 4.694$$

$$k_3 R = 7.854$$

$$k_4 R = 10.995$$

The natural frequencies of the nonrotating uniform beam are given by

$$\omega_i = \left(\frac{k_i R}{R}\right)^2 \left(\frac{EI}{m}\right)^{1/2} \tag{A15}$$

Solving for the constants $C_1, \ldots, C_4$ in equation (A13) gives the following general equation for the mode shapes of the nonrotating cantilever beam:

$$X_i(x) = \sin k_i x + \sinh k_i x + \alpha_i\left(\cos k_i x + \cosh k_i x\right) \tag{A16}$$

where

$$\alpha_i = -\left(\frac{\sinh k_i R + \sin k_i R}{\cosh k_i R + \cos k_i R}\right) \tag{A17}$$

The first four α_i coefficients are

$$\alpha_1 = -1.36222$$

$$\alpha_2 = -0.98187$$

$$\alpha_3 = -1.00078$$

$$\alpha_4 = -0.99997$$

APPENDIX

The following integral property of the normal modes is utilized to simplify equation (A12):

First,

$$\int_0^R X_i^2(x)\,dx = \alpha_i^2 R \tag{A18}$$

Therefore,

$$\ddot{\varphi}_i(t) + \frac{\int_0^R C(x)X_i^2(x)\,dx}{m\alpha_i^2 R}\,\dot{\varphi}_i(t) + \omega_i^2\varphi_i(t) = \frac{P(t)X_i(d)}{m\alpha_i^2 R} \tag{A19}$$

As in reference 14, if zero initial conditions are assumed, the general solution of equation (A19) is

$$\varphi_{id}(t) = \frac{g}{\alpha_i^2\omega_{id}}\int_0^{t_1} q(t)X_i(d)e^{-\nu_i\omega_i(t_1-t)}\sin\omega_{id}(t_1 - t)\,dt \tag{A20}$$

which is the superposition, or Duhamel, integral where

$$q(t) = \frac{P(t)}{mRg} \tag{A21}$$

which is the ratio of the magnitude of the applied concentrated force to the weight of the uniform beam. The damping ratio ν_i in equation (A20) is

$$\nu_i = \frac{\int_0^R C(x)X_i^2(x)\,dx}{2\omega_i m\alpha_i^2 R} \tag{A22}$$

Also,

$$\omega_{id} = \left(1 - \nu_i^2\right)^{1/2}\omega_i \tag{A23}$$

and

$$X_i(d) = \sin\left(\frac{k_i R}{R}\right)d + \sinh\left(\frac{k_i R}{R}\right)d + \alpha_i\left[\cos\left(\frac{k_i R}{R}\right)d + \cosh\left(\frac{k_i R}{R}\right)d\right] \tag{A24}$$

APPENDIX

If the force $P(t)$ is moving along the length of the beam, it produces vibrations that can be calculated by letting v denote the constant velocity at which the force moves along the beam, starting at the free end of the beam, $x = 0$, at time $t = 0$. At any time t, the position of the force on the beam will be

$$d = vt \tag{A25}$$

Under these conditions, equation (A20) becomes

$$\varphi_{id}(t) = \frac{g}{\alpha_i^2 \omega_{id}} \int_0^{t_1} q(t) X_i(vt) e^{-\nu_i \omega_i (t_1 - t)} \sin \omega_{id}(t_1 - t)\, dt \tag{A26}$$

where the modal displacement of the point of application of the moving force is

$$X_i(vt) = \sin a_i t + \sinh a_i t + \alpha_i(\cos a_i t + \cosh a_i t) \tag{A27}$$

where

$$a_i = \frac{k_i R}{R} v \tag{A28}$$

The moving force is considered to vary linearly in magnitude as illustrated in figure 6 where

$$q(t) = q_o\left(1 + \frac{\epsilon}{\tau} t\right) \qquad (0 < t < \tau)$$

$$q(t) = 0 \qquad (\tau < t)$$

and ϵ is the nondimensional rate of change of the applied force with time; thus,

$$\epsilon = \left[\frac{\Delta q(t)}{q_o}\right]\left(\frac{\Delta t}{\tau}\right)^{-1} \tag{A29}$$

The time interval τ corresponds to the time required for the concentrated force to move from the free end of the beam to the fixed end; namely,

$$\tau = \frac{R}{v} \tag{A30}$$

APPENDIX

The final equations for the mode participation factors for the damped response to a moving force are as follows:

For $0 < t < \tau$,

$$\varphi_{id}(t) = \frac{q_o g}{\alpha_i^2 \omega_{id}} \int_0^{t_1} \left(1 + \frac{\epsilon}{\tau} t\right) X_i(vt) e^{-\nu_i \omega_i (t_1 - t)} \sin \omega_{id}(t_1 - t)\, dt \tag{A31}$$

For $\tau < t$,

$$\varphi_{id}(t) = \frac{q_o g}{\alpha_i^2 \omega_{id}} \int_0^{\tau} \left(1 + \frac{\epsilon}{\tau} t\right) X_i(vt) e^{-\nu_i \omega_i (t_1 - t)} \sin \omega_{id}(t_1 - t)\, dt \tag{A32}$$

Rotating Blade

In order to obtain a first approximation of the response of the rotating helicopter blade to a radially moving force, the preceding analysis is used by substituting rotating blade natural frequencies. These frequencies are obtained from reference 19, where the rotating blade natural frequencies are determined from

$$\omega_{iR}^2 = \omega_i^2 + K_i \Omega^2$$

The appropriate Southwell coefficients K_i are selected from reference 19 for the flapwise and chordwise bending modes. Also,

$$\omega_{idR} = \left(1 - \nu_i^2\right)^{1/2} \omega_{iR} \tag{A33}$$

where the values of effective damping ratio ν_i are assigned.

Using the rotating-blade natural frequencies ω_{iR} and expanding, integrating, and recombining terms from equations (A31) and (A32) results in the following approximate equations for the rotating blade mode participation factors $\varphi_{idR}(t_1)$:

APPENDIX

For $0 < t_1 < \tau$,

$$\varphi_{idR}(t_1) \approx \frac{q_0 g}{2\alpha_i^2 \omega_{idR}} \Bigg(\Big[\Big(1 + \frac{\epsilon}{\tau} t_1\Big)\big(C_{i,0,1} - \bar{C}_{i,0,1}\big) - \frac{\epsilon}{\tau}\big(C_{i,\epsilon,1} - \bar{C}_{i,\epsilon,1}\big) \Big] \sin a_i t_1 + \Big[\Big(1 + \frac{\epsilon}{\tau} t_1\Big)\big(C_{i,0,2} - \bar{C}_{i,0,2}\big) - \frac{\epsilon}{\tau}\big(C_{i,\epsilon,2} - \bar{C}_{i,\epsilon,2}\big) \Big] \cos a_i t_1$$
$$+ \Big[\Big(1 + \frac{\epsilon}{\tau} t_1\Big) C_{i,0,4} - \frac{\epsilon}{\tau} C_{i,\epsilon,4} \Big] e^{a_i t_1} - \Big[\Big(1 + \frac{\epsilon}{\tau} t_1\Big) \bar{C}_{i,0,4} - \frac{\epsilon}{\tau} \bar{C}_{i,\epsilon,4} \Big] e^{-a_i t_1} + e^{-\nu_i \omega_{iR} t_1} \Bigg\{ \Big[C_{i,0,1} + \bar{C}_{i,0,1} - C_{i,0,3} + \bar{C}_{i,0,3}$$
$$- \frac{\epsilon}{\tau}\big(C_{i,\epsilon,1} + \bar{C}_{i,\epsilon,1} - C_{i,\epsilon,3} + \bar{C}_{i,\epsilon,3}\big) \Big] \sin \omega_{idR} t_1 - \Big[C_{i,0,2} - \bar{C}_{i,0,2} + C_{i,0,4} - \bar{C}_{i,0,4}$$
$$- \frac{\epsilon}{\tau}\big(C_{i,\epsilon,2} - \bar{C}_{i,\epsilon,2} + C_{i,\epsilon,4} - \bar{C}_{i,\epsilon,4}\big) \Big] \cos \omega_{idR} t_1 \Bigg\} \Bigg) \qquad \text{(A34)}$$

For $\tau < t_1$,

$$\varphi_{idR}(t_1) \approx \frac{q_0 g}{2\alpha_i^2 \omega_{idR}} \Bigg[e^{-\nu_i \omega_{iR}(t_1 - \tau)} \Bigg(\Big[(1+\epsilon) C_{i,0,1} - \frac{\epsilon}{\tau} C_{i,\epsilon,1} \Big] \sin \Big[a_i \tau - \omega_{idR}(t_1 - \tau) \Big] + \Big[(1+\epsilon) C_{i,0,2} - \frac{\epsilon}{\tau} C_{i,\epsilon,2} \Big] \cos \Big[a_i \tau - \omega_{idR}(t_1 - \tau) \Big]$$
$$- \Big[(1+\epsilon) \bar{C}_{i,0,1} - \frac{\epsilon}{\tau} \bar{C}_{i,\epsilon,1} \Big] \sin \Big[a_i \tau + \omega_{idR}(t_1 - \tau) \Big] - \Big[(1+\epsilon) \bar{C}_{i,0,2} - \frac{\epsilon}{\tau} C_{i,\epsilon,2} \Big] \cos \Big[a_i \tau + \omega_{idR}(t_1 - \tau) \Big]$$
$$+ \Big\{ \Big[(1+\epsilon) C_{i,0,3} - \frac{\epsilon}{\tau} C_{i,\epsilon,3} \Big] e^{a_i \tau} - \Big[(1+\epsilon) \bar{C}_{i,0,3} - \frac{\epsilon}{\tau} C_{i,\epsilon,3} \Big] e^{-a_i \tau} \Big\} \sin \omega_{idR}(t_1 - \tau)$$
$$+ \Big\{ \Big[(1+\epsilon) C_{i,0,4} - \frac{\epsilon}{\tau} C_{i,\epsilon,4} \Big] e^{a_i \tau} - \Big[(1+\epsilon) \bar{C}_{i,0,4} - \frac{\epsilon}{\tau} \bar{C}_{i,\epsilon,4} \Big] e^{-a_i \tau} \Big\} \cos \omega_{idR}(t_1 - \tau) \Bigg)$$
$$+ e^{-\nu_i \omega_{iR} t_1} \Bigg\{ \Big[C_{i,0,1} + \bar{C}_{i,0,1} - C_{i,0,3} + C_{i,0,3} - \frac{\epsilon}{\tau}\big(C_{i,\epsilon,1} + \bar{C}_{i,\epsilon,1} - C_{i,\epsilon,3} + \bar{C}_{i,\epsilon,3}\big) \Big] \sin \omega_{idR} t_1$$
$$- \Big[C_{i,0,2} - C_{i,0,2} + C_{i,0,4} - \bar{C}_{i,0,4} - \frac{\epsilon}{\tau}\big(C_{i,\epsilon,2} - \bar{C}_{i,\epsilon,2} + C_{i,\epsilon,4} - \bar{C}_{i,\epsilon,4}\big) \Big] \cos \omega_{idR} t_1 \Bigg\} \Bigg] \qquad \text{(A35)}$$

The coefficients in equations (A34) and (A35) are as follows:

$$\left.\begin{aligned}
C_{i,0,1} &= \frac{B_i - \alpha_i A_i}{A_i^2 + B_i^2} & \bar{C}_{i,0,1} &= \frac{\bar{B}_i - \alpha_i A_i}{A_i^2 + \bar{B}_i^2} \\
C_{i,0,2} &= \frac{A_i + \alpha_i B_i}{A_i^2 + B_i^2} & \bar{C}_{i,0,2} &= \frac{A_i + \alpha_i \bar{B}_i}{A_i^2 + \bar{B}_i^2} \\
C_{i,0,3} &= \frac{(1 + \alpha_i) E_i}{E_i^2 + D_i^2} & \bar{C}_{i,0,3} &= \frac{(1 - \alpha_i) \bar{E}_i}{\bar{E}_i^2 + D_i^2} \\
C_{i,0,4} &= \frac{(1 + \alpha_i) D_i}{E_i^2 + D_i^2} & \bar{C}_{i,0,4} &= \frac{(1 - \alpha_i) D_i}{\bar{E}_i^2 + D_i^2}
\end{aligned}\right\} \qquad \text{(A36)}$$

APPENDIX

$$
\left.
\begin{aligned}
C_{i,\epsilon,1} &= \frac{2A_iB_i - \left(A_i^2 - B_i^2\right)\alpha_i}{\left(A_i^2 + B_i^2\right)^2} & \overline{C}_{i,\epsilon,1} &= \frac{2A_i\overline{B}_i - \left(A_i^2 - \overline{B}_i^2\right)\alpha_i}{\left(A_i^2 + \overline{B}_i^2\right)^2} \\
C_{i,\epsilon,2} &= \frac{\left(A_i^2 - B_i^2\right) + 2\alpha_iA_iB_i}{\left(A_i^2 + B_i^2\right)^2} & \overline{C}_{i,\epsilon,2} &= \frac{\left(A_i^2 - \overline{B}_i^2\right) + 2\alpha_iA_i\overline{B}_i}{\left(A_i^2 + \overline{B}_i^2\right)^2} \\
C_{i,\epsilon,3} &= \frac{\left(E_i^2 - D_i^2\right)\left(1 + \alpha_i\right)}{\left(E_i^2 + D_i^2\right)^2} & \overline{C}_{i,\epsilon,3} &= \frac{\left(\overline{E}_i^2 - D_i^2\right)\left(1 - \alpha_i\right)}{\left(\overline{E}_i^2 + D_i^2\right)^2} \\
C_{i,\epsilon,4} &= \frac{2E_iD_i\left(1 + \alpha_i\right)}{\left(E_i^2 + D_i^2\right)^2} & \overline{C}_{i,\epsilon,4} &= \frac{2\overline{E}_iD_i\left(1 - \alpha_i\right)}{\left(\overline{E}_i^2 + D_i^2\right)^2}
\end{aligned}
\right\} \tag{A37}
$$

where

$$
\left.
\begin{aligned}
A_i &= \nu_i\omega_{iR} \\
B_i &= a_i + \omega_{idR} \\
\overline{B}_i &= a_i - \omega_{idR} \\
E_i &= a_i + \nu_i\omega_{iR} \\
\overline{E}_i &= -a_i + \nu_i\omega_{iR} \\
D_i &= \omega_{idR}
\end{aligned}
\right\} \tag{A38}
$$

Some of the response characteristics can be deduced directly from the undamped-blade equations of motion. This equation is given as follows for a constant force:

For $\nu_i = 0$, $\epsilon = 0$, and $0 < t_1 < \tau$,

$$
\begin{aligned}
\varphi_{iR}\left(t_1\right) \approx \frac{q_0g}{\alpha_i^2\left(a_i^4 - \omega_{iR}^4\right)}\Big\{&\left(a_i^2 - \omega_{iR}^2\right)\sinh a_it_1 - \left(a_i^2 + \omega_{iR}^2\right)\sin a_it_1 \\
&+ \alpha_i\left[\left(a_i^2 - \omega_{iR}^2\right)\cosh a_it_1 - \left(a_i^2 + \omega_{iR}^2\right)\cos a_it_1\right] \\
&+ 2a_i\omega_{iR}\sin \omega_{iR}t_1 + 2\alpha_i\omega_{iR}^2\cos \omega_{iR}t_1\Big\}
\end{aligned} \tag{A39}
$$

APPENDIX

For $\tau < t_1$,

$$\varphi_{iR}(t_1) \approx \frac{q_o g}{2\alpha_i^2 \omega_{iR}} \left(\frac{1}{a_i + \omega_{iR}} \left\{ \sin\left[a_i\tau - \omega_{iR}(t_1 - \tau)\right] + \alpha_i \cos\left[a_i\tau - \omega_{iR}(t_1 - \tau)\right] \right\} \right.$$

$$- \frac{1}{a_i - \omega_{iR}} \left\{ \sin\left[a_i\tau + \omega_{iR}(t_1 - \tau)\right] + \alpha_i \cos\left[a_i\tau + \omega_{iR}(t_1 - \tau)\right] \right\}$$

$$+ \frac{1}{a_i^2 + \omega_{iR}^2} \left\{ \left[(1 + \alpha_i)e^{a_i\tau} + (1 - \alpha_i)e^{-a_i\tau}\right] a_i \sin \omega_{iR}(t_1 - \tau) \right.$$

$$\left. + \left[(1 + \alpha_i)e^{a_i\tau} - (1 - \alpha_i)e^{-a_i\tau}\right] \omega_{iR} \cos \omega_{iR}(t_1 - \tau) \right\}$$

$$\left. + \frac{2\omega_{iR}}{a_i^4 - \omega_{iR}^4} \left(a_i \omega_{iR} \sin \omega_{iR} t_1 + \alpha_i \omega_{iR}^2 \cos \omega_{iR} t_1\right) \right) \qquad \text{(A40)}$$

If the velocity v of the moving force on a nonrotating beam is very small, the equations of motion for $t = 0$ reduce to the static displacement of the free end of a cantilever beam subjected to a concentrated load at the tip as follows:

$$y = \sum_{i=1}^{n} \varphi_i(t_1) X_i(x)$$

and equation (A39) becomes, for the forced, nonrotating blade,

$$\varphi_i(t_1) = \frac{q_o g}{\alpha_i^2 (a_i^4 - \omega_i^4)} \left\{ (a_i^2 - \omega_i^2) \sinh a_i t_1 - (a_i^2 + \omega_i^2) \sin a_i t_1 \right.$$

$$\left. + \alpha_i \left[(a_i^2 - \omega_i^2) \cosh a_i t_1 - (a_i^2 + \omega_i^2) \cos a_i t_1 \right] \right\}$$

For $t_1 = 0$, $v = 0$,

$$\varphi_i(0) = \frac{2q_o g}{\alpha_i \omega_i^2} = \frac{2P}{\alpha_i R m \omega_i^2}$$

$$y = \sum_{i=1}^{n} \varphi_i(0) X_i(0)$$

$$= \sum_{i=1}^{n} \frac{2P}{Rm\omega_i^2} \left(\frac{X_i(0)}{\alpha_i} \right)$$

$$= \frac{4PR^3}{EI} \sum_{i=1}^{n} \frac{1}{(k_i R)^4}$$

$$= \frac{4PR^3}{EI} \left[\frac{1}{(1.875)^4} + \frac{1}{(4.694)^4} + \frac{1}{(7.855)^4} + \ldots \right]$$

$$= \frac{4PR^3}{EI} (0.08071 + 0.00206 + 0.00026 + \ldots)$$

$$= 0.3321 \frac{PR^3}{EI}$$

The exact value for the static tip deflection is

$$y = \frac{PR^3}{3EI}$$

With three terms of the series the error is less than 0.5 percent.

The following general equations give the approximate values of beam deflection, slope, bending moment, and shear:

$$\left.\begin{aligned} y(x,t_1) &\approx \sum_{i=1}^{n} \varphi_i(t_1) X_i(x) \\ \theta(x,t_1) &\approx \sum_{i=1}^{n} \varphi_i(t_1) X'(x) \\ M(x,t_1) &\approx -EI \sum_{i=1}^{n} \varphi_i(t_1) X_i''(x) \\ V(x,t_1) &\approx -EI \sum_{i=1}^{n} \varphi_i(t_1) X_i'''(x) \end{aligned}\right\} \quad \text{(A41)}$$

where

$$\left.\begin{aligned} X_i'(x) &= k_i\left[\cosh k_i x + \cos k_i x + \alpha_i\left(\sinh k_i x - \sin k_i x\right)\right] \\ X''(x) &= k_i^2\left[\sinh k_i x - \sin k_i x + \alpha_i\left(\cosh k_i x - \cos k_i x\right)\right] \\ X'''(x) &= k_i^3\left[\cosh k_i x - \cos k_i x + \alpha_i\left(\sinh k_i x + \sin k_i x\right)\right] \end{aligned}\right\} \qquad \text{(A42)}$$

REFERENCES

1. Scheiman, James; and Ludi, LeRoy H.: Qualitative Evaluation of Effect of Helicopter Rotor-Blade Tip Vortex On Blade Airloads. NASA TN D-1637, 1963.

2. Leverton, John W.: Helicopter Noise – Blade Slap. Part 1: Review and Theoretical Study. NASA CR-1221, 1968.

3. Miller, R. H.: A Discussion of Rotor Blade Harmonic Airloading. CAL/TRECOM Symposium Proceedings Vol. I – Dynamic Load Problems Associated With Helicopters and V/STOL Aircraft, June 1963.

4. Piziali, Raymond A.; and DuWaldt, Frank A.: A Method for Computing Rotary Wing Airload Distributions in Forward Flight. TCREC Tech. Rep. 62-44, U.S. Army, Nov. 1962.

5. Tararine, S.: Experimental and Theoretical Study of Local Induced Velocities Over a Rotor Disc. CAL/TRECOM Symposium Proceedings Vol. I – Dynamic Load Problems Associated With Helicopters and V/STOL Aircraft, June 1963.

6. Scully, Michael P.: Approximate Solutions for Computing Helicopter Harmonic Airloads. ASRL Tech. Rep. 123-2 (Contract NOw 64-0188-d), Massachusetts Inst. Technol., Dec. 1965.

7. Davenport, Franklyn J.: A Method for Computation of the Induced Velocity Field of a Rotor in Forward Flight, Suitable for Application to Tandem Rotor Configuration. J. Amer. Helicopter Soc., vol. 9, no. 3, July 1964, pp. 26-33.

8. Huston, Robert J.: Wind-Tunnel Measurements of Performance, Blade Motions, and Blade Air Loads for Tandem-Rotor Configurations With and Without Overlap. NASA TN D-1971, 1963.

9. Pruyn, R. R.; and Alexander, W. T., Jr.: The USAAVLABS Tandem Rotor Airloads Measurement Program. AIAA Paper No. 66-735, Sept. 1966.

10. Jenney, David S.; Olson, John R.; and Landgrebe, Anton John: A Reassessment of Rotor Hovering Performance Prediction Methods. No. 100, 23rd Annual National Forum Proceedings, Amer. Helicopter Soc., Inc., May 1967.

11. Drees, Jan M.: Aeroelastic Rotor Phenomena and Nonsteady Rotor Aerodynamics. International Congress on Subsonic Aeronautics. Ann. N.Y. Acad. Sci., vol. 154, art. 2, Nov. 22, 1968, pp. 481-505.

12. Lynn, Robert R.; and Drees, Jan M.: Promise of Compounding. J. Amer. Helicopter Soc., vol. 12, no. 1, Jan. 1967, pp. 1-20.

13. Simons, I. A.: Some Aspects of Blade/Vortex Interaction on Helicopter Rotors in Forward Flight. J. Sound Vib., vol. 4, no. 3, Nov. 1966, pp. 268-281.

14. Timoshenko, S.; and Young, D. H.: Vibration Problems in Engineering. Third ed., D. Van Nostrand Co., Inc. c.1955.

15. Inglis, C. E.: A Mathematical Treatise on Vibrations in Railway Bridges. Cambridge Univ. Press, 1934.

16. Bishop, R. E. D.; and Johnson, D. C.: The Mechanics of Vibration. Cambridge Univ. Press, 1960.

17. Park, W. H.: Mass-Spring-Damper Response to Repetitive Impact. Trans. ASME, Ser. B: J. Eng. Ind., vol. 89, no. 4, Nov. 1967, pp. 587-596.

18. Paul, William F.: A Self-Excited Rotor Blade Oscillation at High Subsonic Mach Numbers. No. 228, 24th Annual National Forum Proceedings, Amer. Helicopter Soc., Inc., May 1968.

19. Yntema, Robert T.: Simplified Procedures and Charts for the Rapid Estimation of Bending Frequencies of Rotating Beams. NACA TN 3459, 1955. (Supersedes NACA RM L54G02.)

20. Lewis, Frank M.: Vibration During Acceleration Through a Critical Speed. Trans. ASME, vol. 54, no. 23, Dec. 1932, pp. 253-261.

TABLE 1.- CANTILEVER-BLADE CHARACTERISTICS

Blade radius, R	17.5 ft (5.35 meters)
Mass per unit length, m	0.130 slug/ft (6.23 kg/meter)
Flapwise structural stiffness, $(EI)_F$	4.86×10^4 lbf-ft^2 (2.01×10^4 newton-meters^2)
Chordwise structural stiffness, $(EI)_C$	2.78×10^6 lbf-ft^2 (1.15×10^6 newton-meters^2)
Number of blades	3
Rotor rotational speed	37 radians/sec
Flapwise mode natural frequencies, rotating:	
First bending mode	41 radians/sec
Second bending mode	102 radians/sec
Third bending mode	194 radians/sec
Fourth bending mode	293 radians/sec
Chordwise natural frequencies, rotating:	
First bending mode	52 radians/sec
Second bending mode	304 radians/sec

All damping coefficients, ν_i, are assigned as noted in specific examples

TABLE 2.- ILLUSTRATIVE EXAMPLES

Blade mode	n	i	ω_{iR}/Ω	ν_i	ϵ	μ	$\Delta\psi$, deg	Figure	Remarks
Flapwise bending	3	1	1.11	0.50	0	0.3	150	8	Single impulse
		2	2.76	.20		.5	100		
		3	5.24	.27		.7	80		
Flapwise bending	3	1	1.11	0.25	0, -1	0.7	80	9	Single impulse
		2	2.76	.10					
		3	5.24	.14					
Chordwise bending	1	1	1.41	0.06	0	0.3	150	10	First rotor revolution and tenth rotor revolution
Chordwise bending	1	1	1.41	0.06	0	0.7	80	11	First rotor revolution and tenth rotor revolution
Flapwise bending	3	1	1.11	0.13	0	0.3	150	12	Single impulse and repetitive impulse
		2	2.76	.05					
		3	5.24	.07					

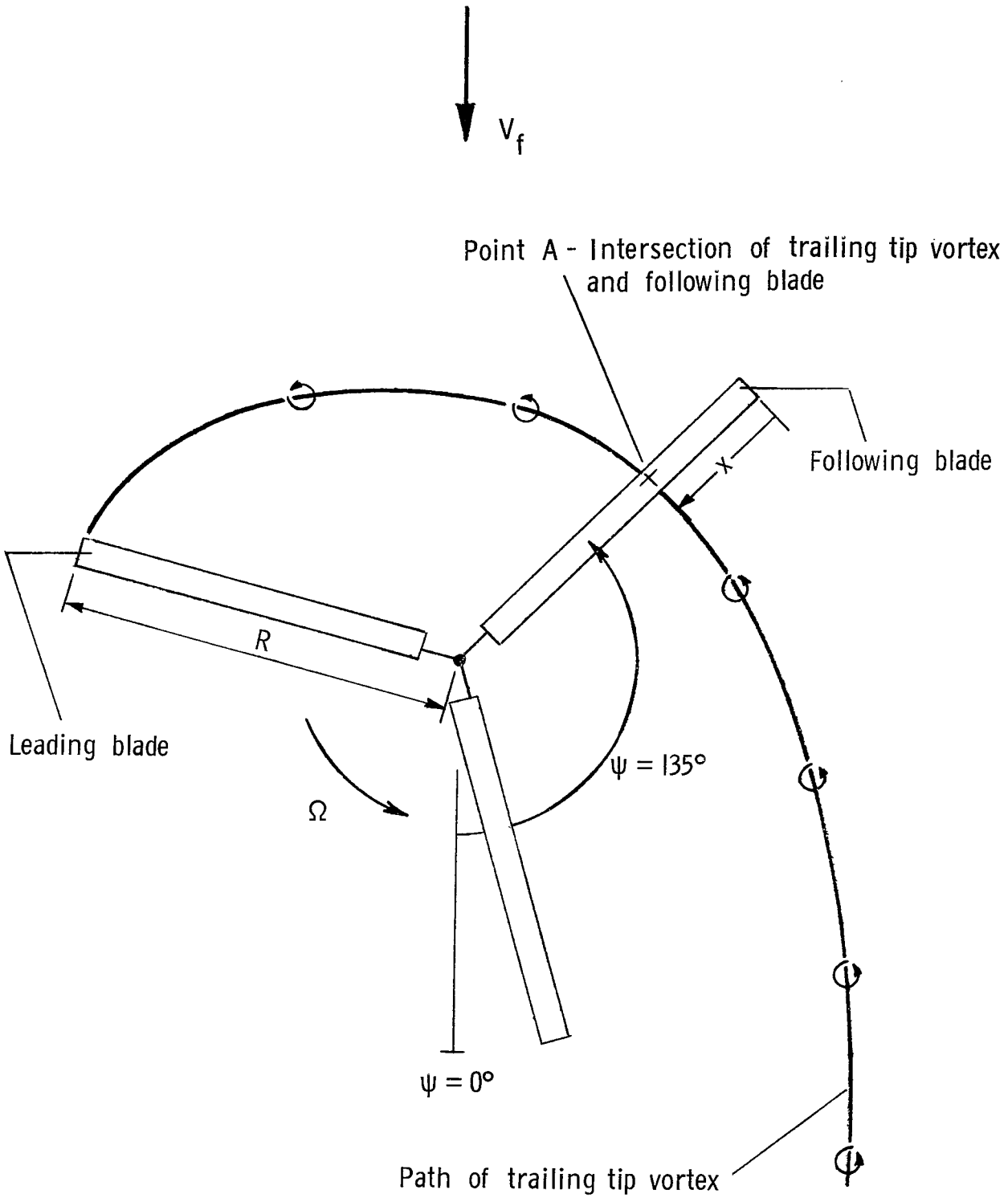

Figure 1.- Intersection of following blade with tip vortex trailed from a leading blade at tip-speed ratio μ of 0.2.

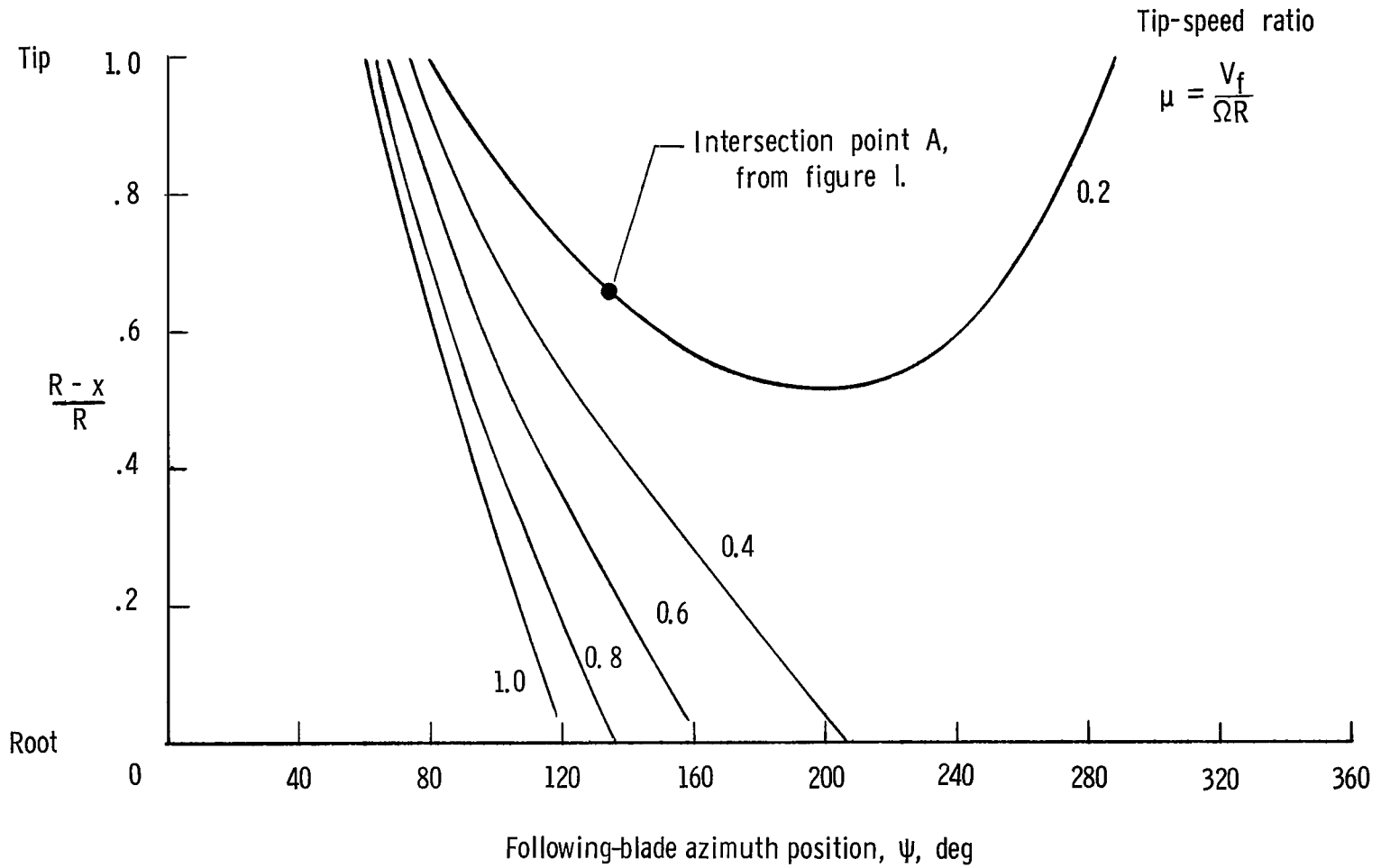

Figure 2.- Vortex-blade intersection point path for various tip-speed ratios. Three-blade rotor; ΩR = 650 feet per second (198 meters per second).

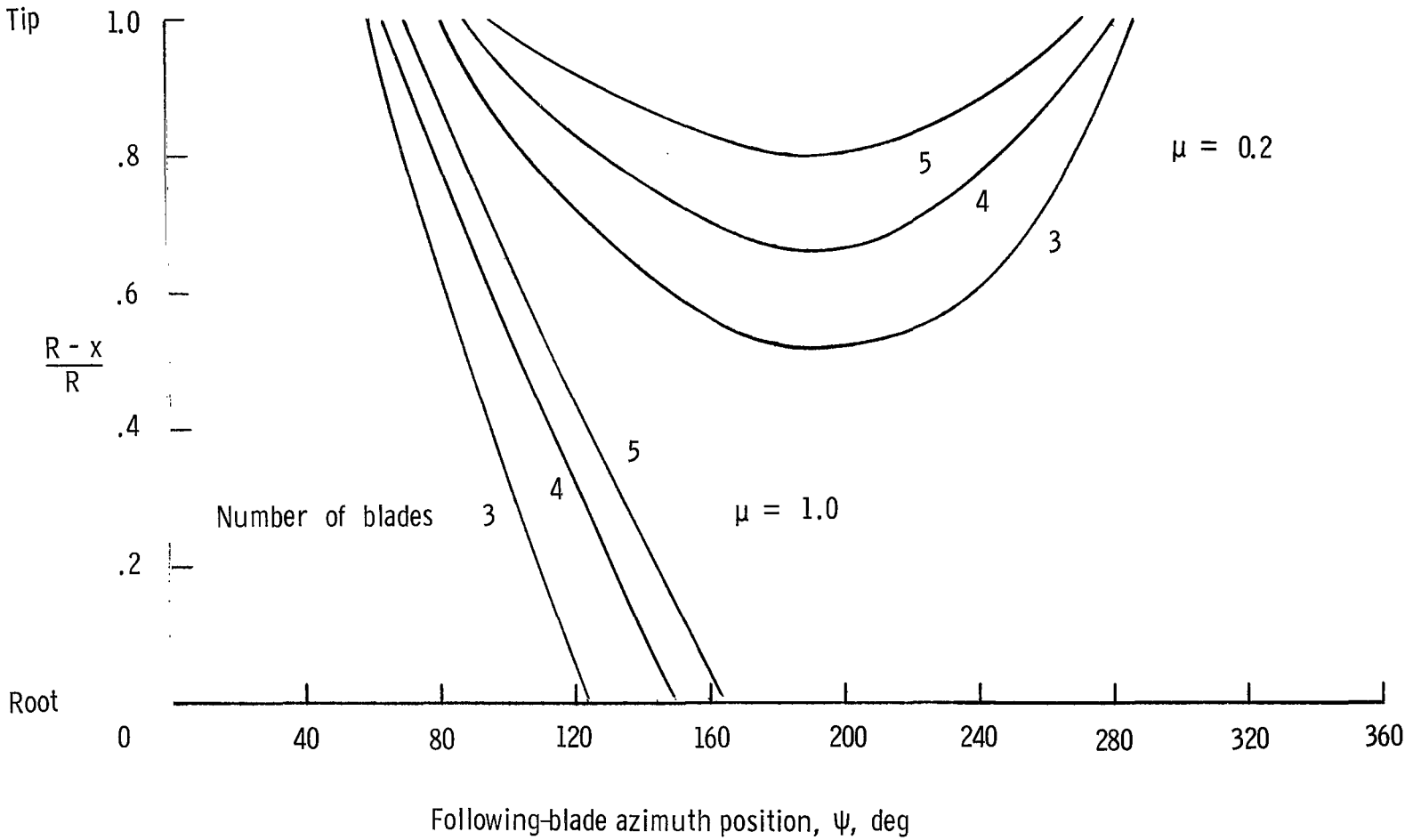

Figure 3.- Vortex-blade intersection point path for various numbers of blades at two tip-speed ratios. ΩR = 650 feet per second (198 meters per second).

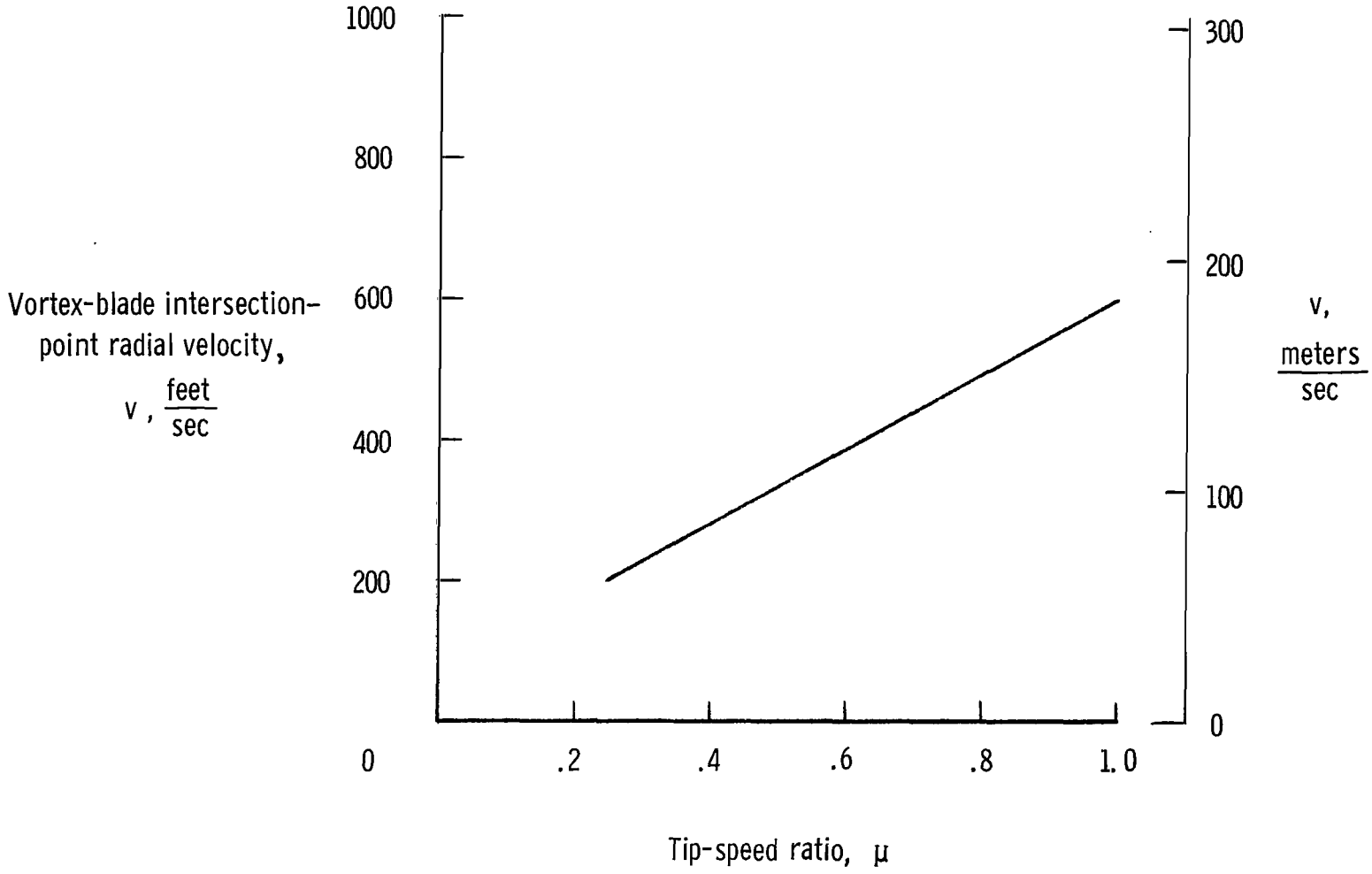

Figure 4.- Radial velocity of vortex-blade intersection point. Three-bladed rotor; ΩR = 650 feet per second (198 meters per second).

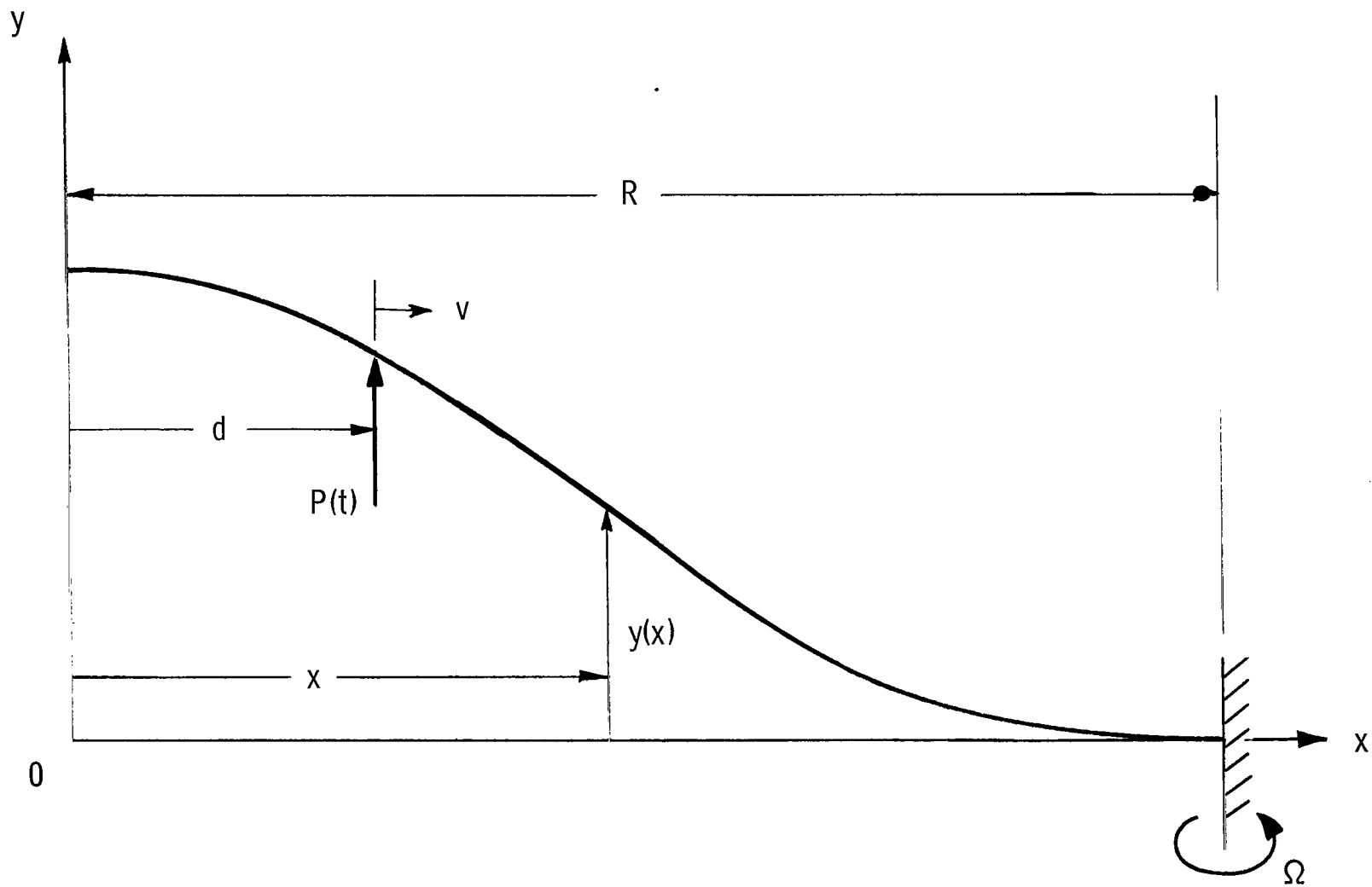

Figure 5.- Rotating cantilever beam with concentrated point loading.

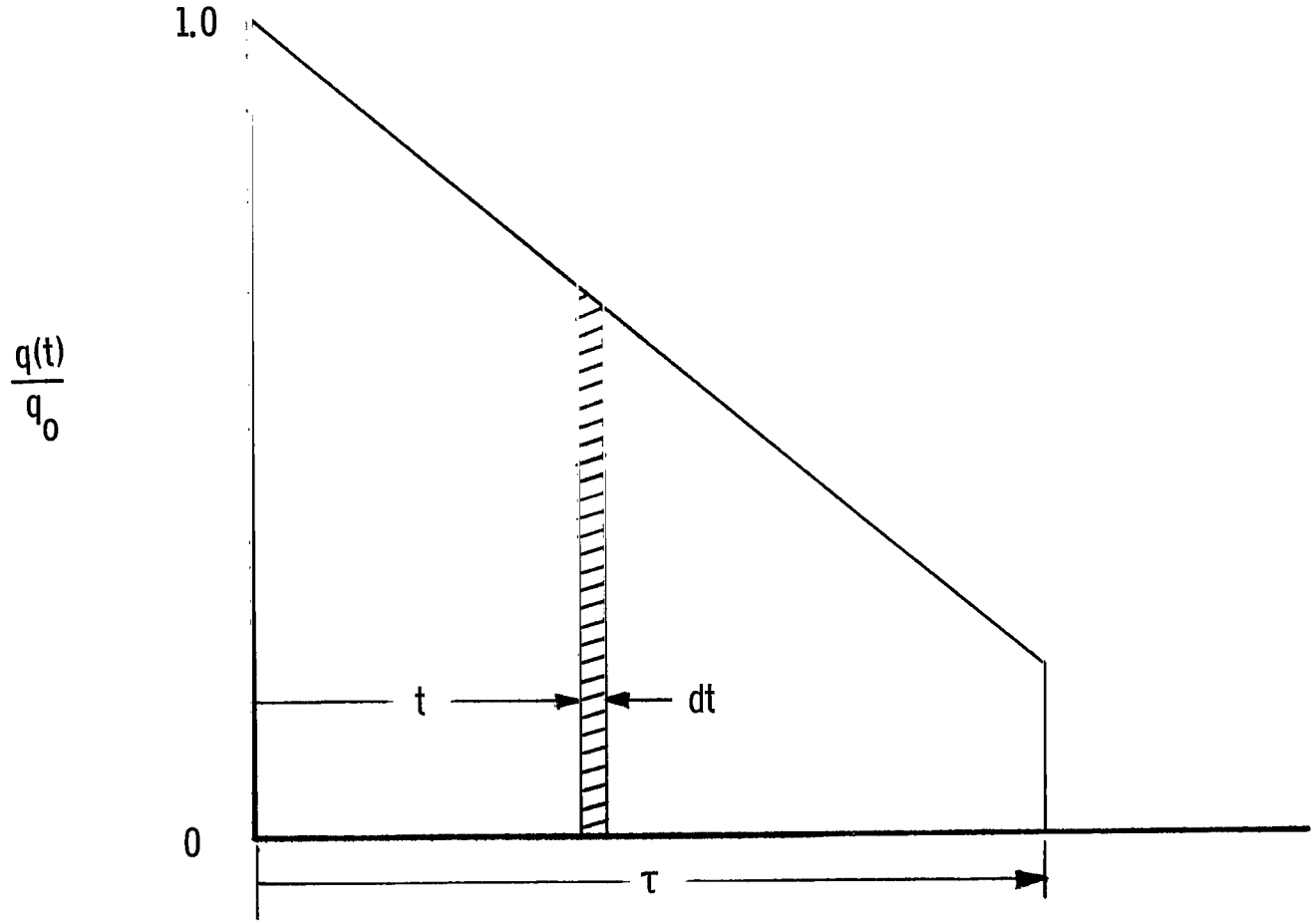

Figure 6.- Loading variation with time.

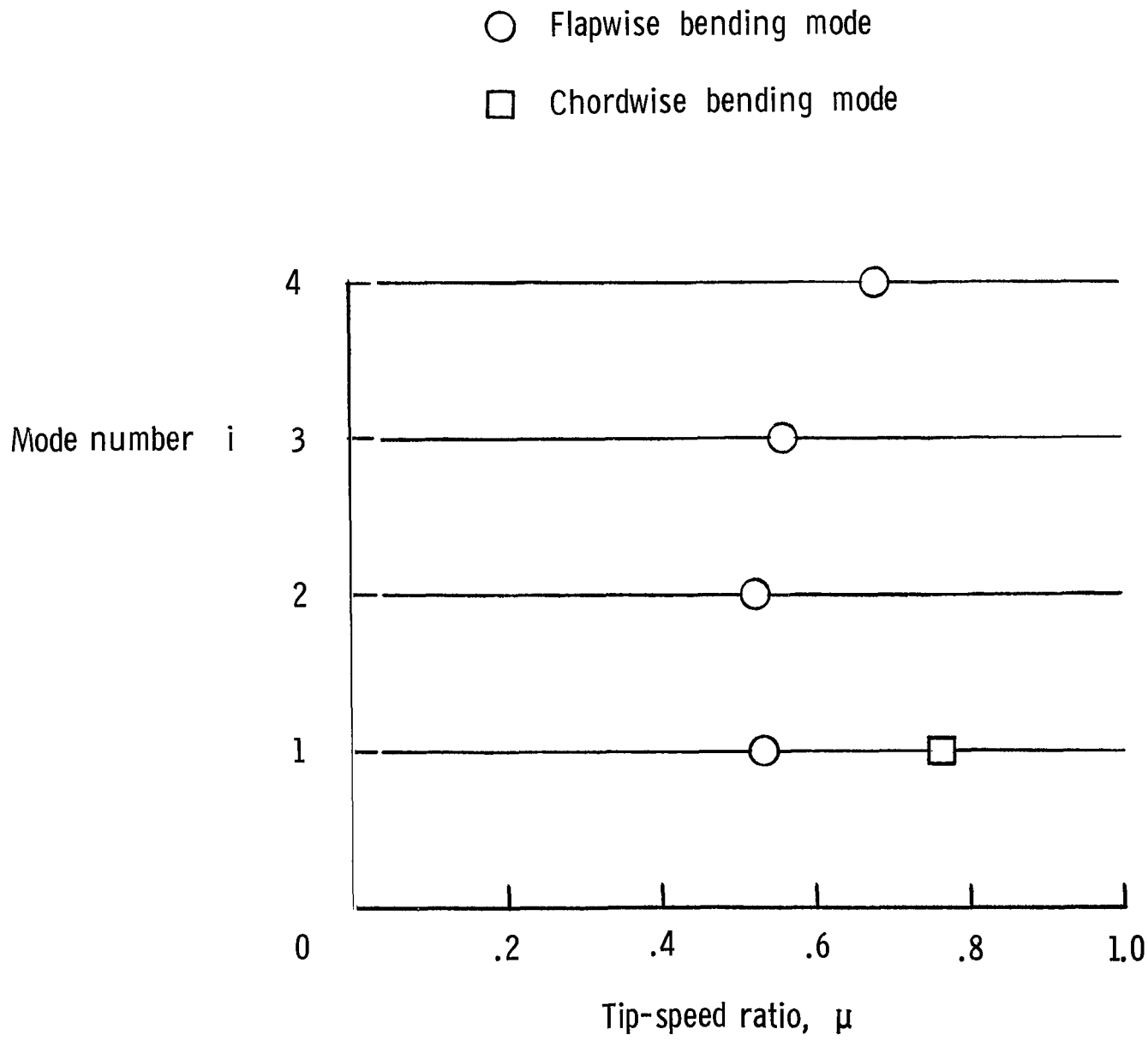

Figure 7.- Critical tip-speed ratios for various blade bending modes of cantilever blade. Three-blade rotor; ΩR = 650 feet per second (198 meters per second).

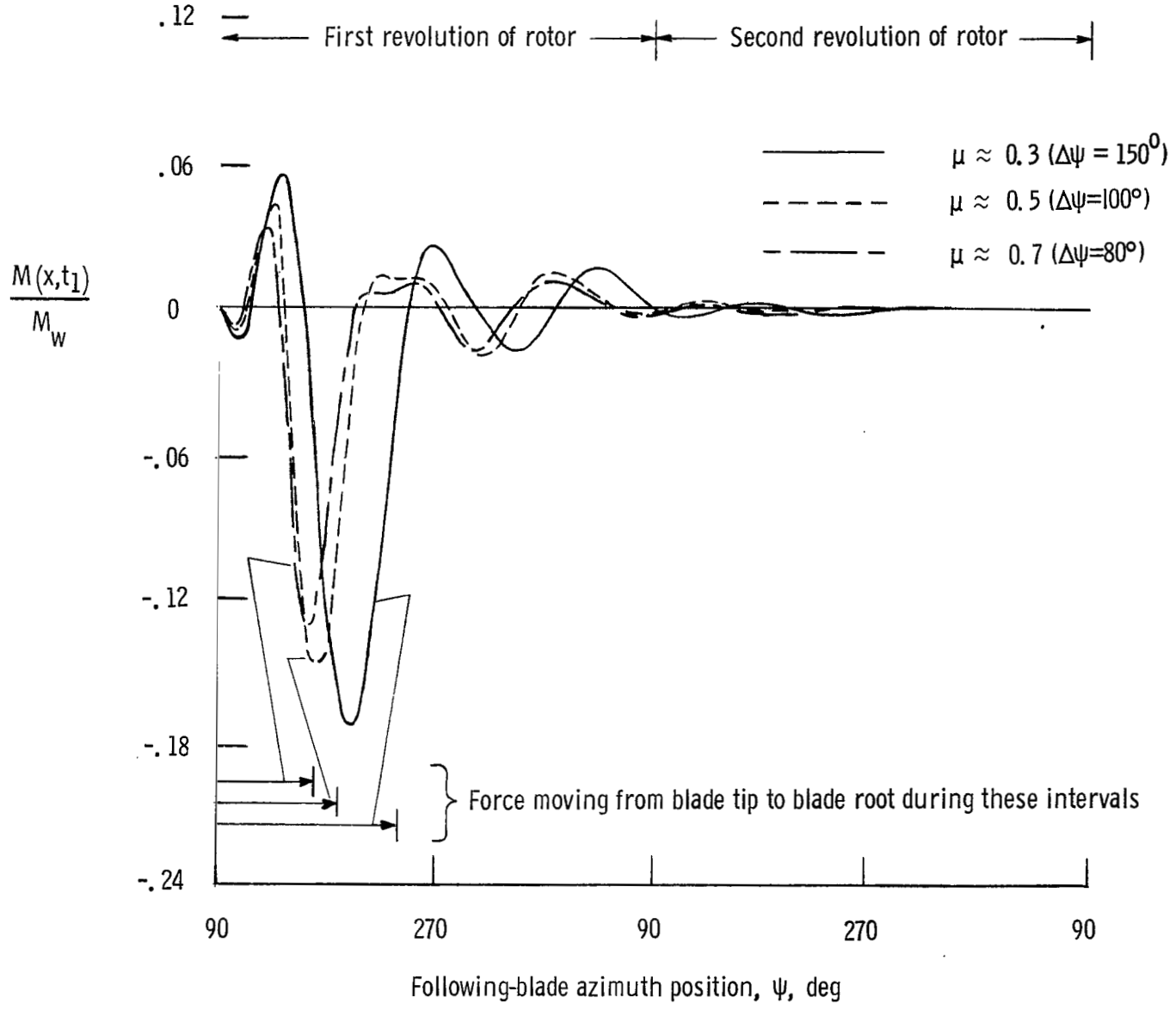

Figure 8.- Blade-root (x = R) flapwise bending moment for a single impulse. Three-blade rotor; n = 3; ε = 0; ν_1 = 0.50; ν_2 = 0.20; ν_3 = 0.27.

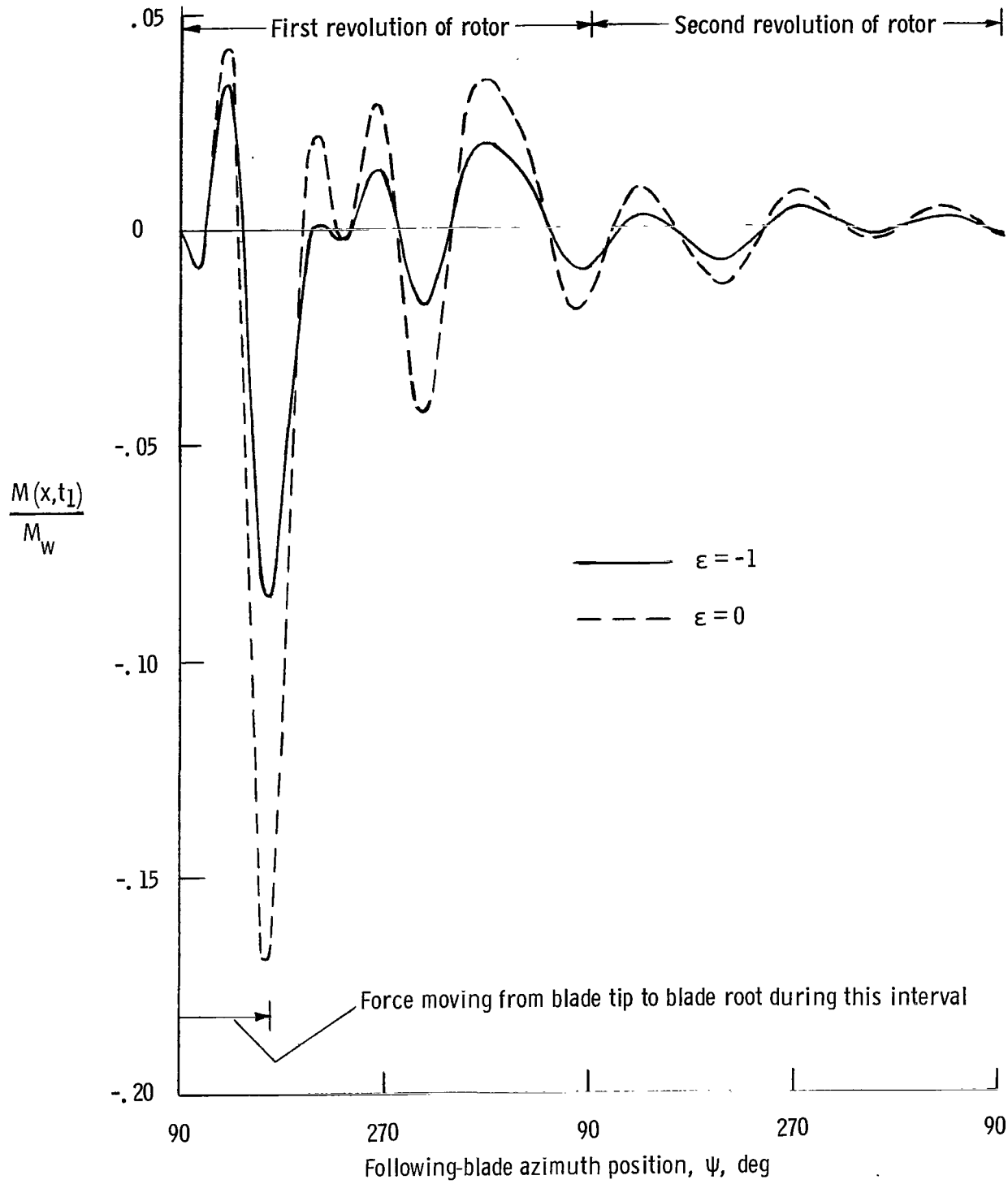

Figure 9.- Blade-root (x = R) flapwise bending moment for a single impulse. Three-blade rotor; $\mu \approx 0.7$ ($\Delta\psi = 80^0$); n = 3; $\nu_1 = 0.25$; $\nu_2 = 0.10$; $\nu_3 = 0.14$.

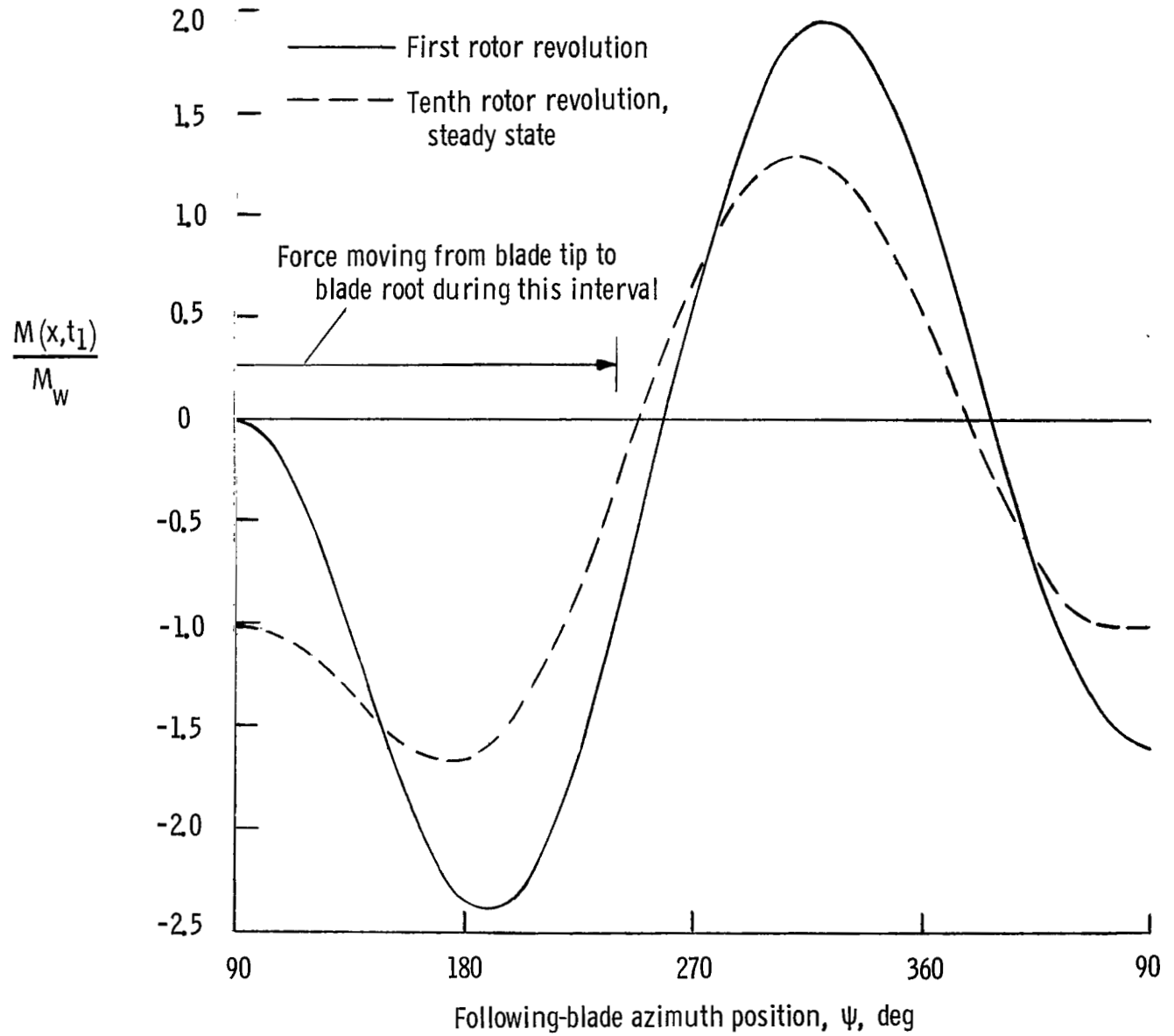

Figure 10.- Blade-root (x = R) chordwise bending moment for single and repetitive impulse. $\varepsilon = 0$; $\mu \approx 0.3$ ($\Delta\psi = 150^0$); three-blade rotor; $n = 1$; $\nu_1 = 0.06$.

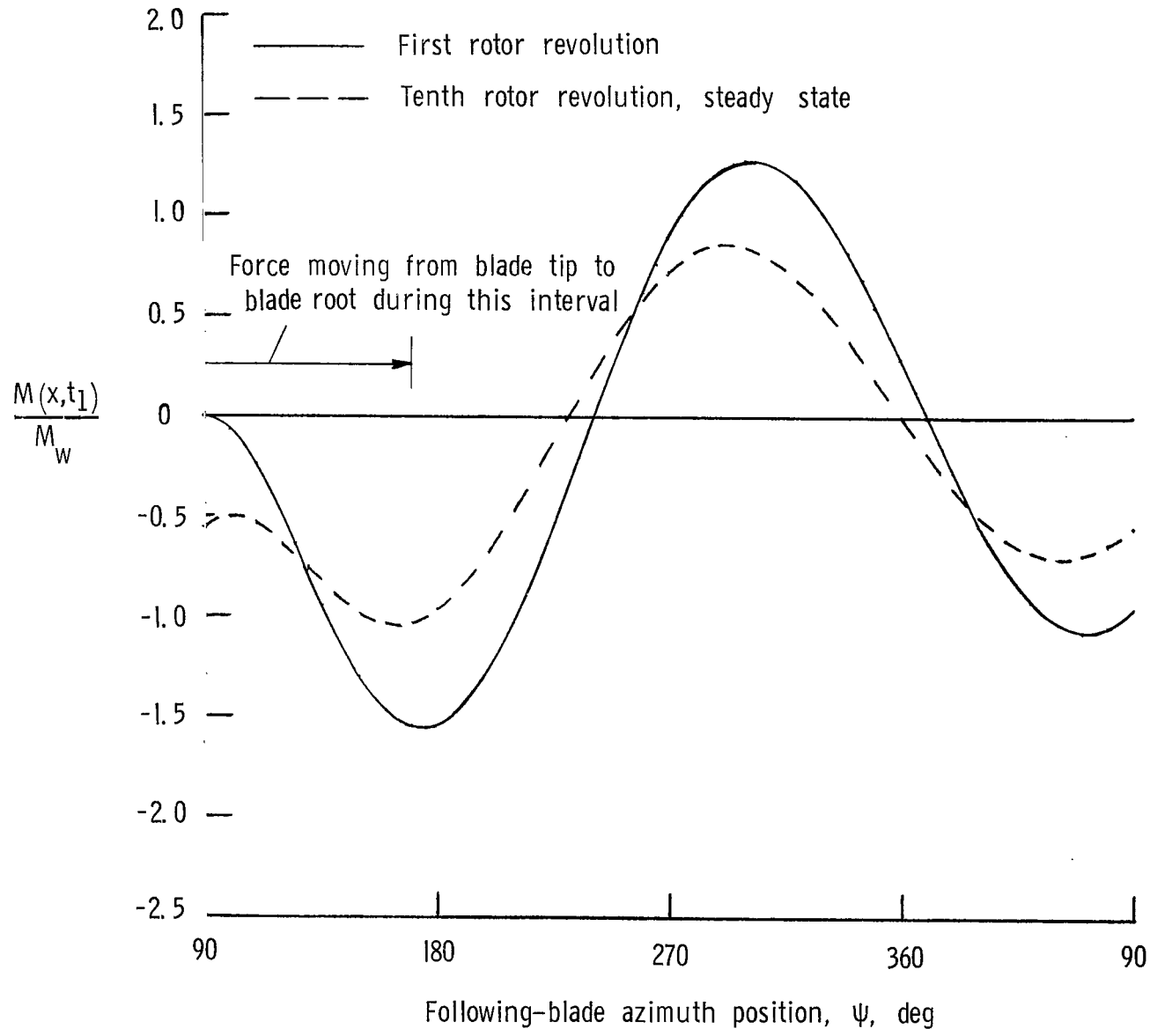

Figure 11.- Blade-root (x = R) chordwise bending moment for single and repetitive impulse. $\varepsilon = 0$; $\mu = 0.7$ ($\Delta\psi = 80^0$); three-blade rotor; $n = 1$; $\nu_1 = 0.06$.

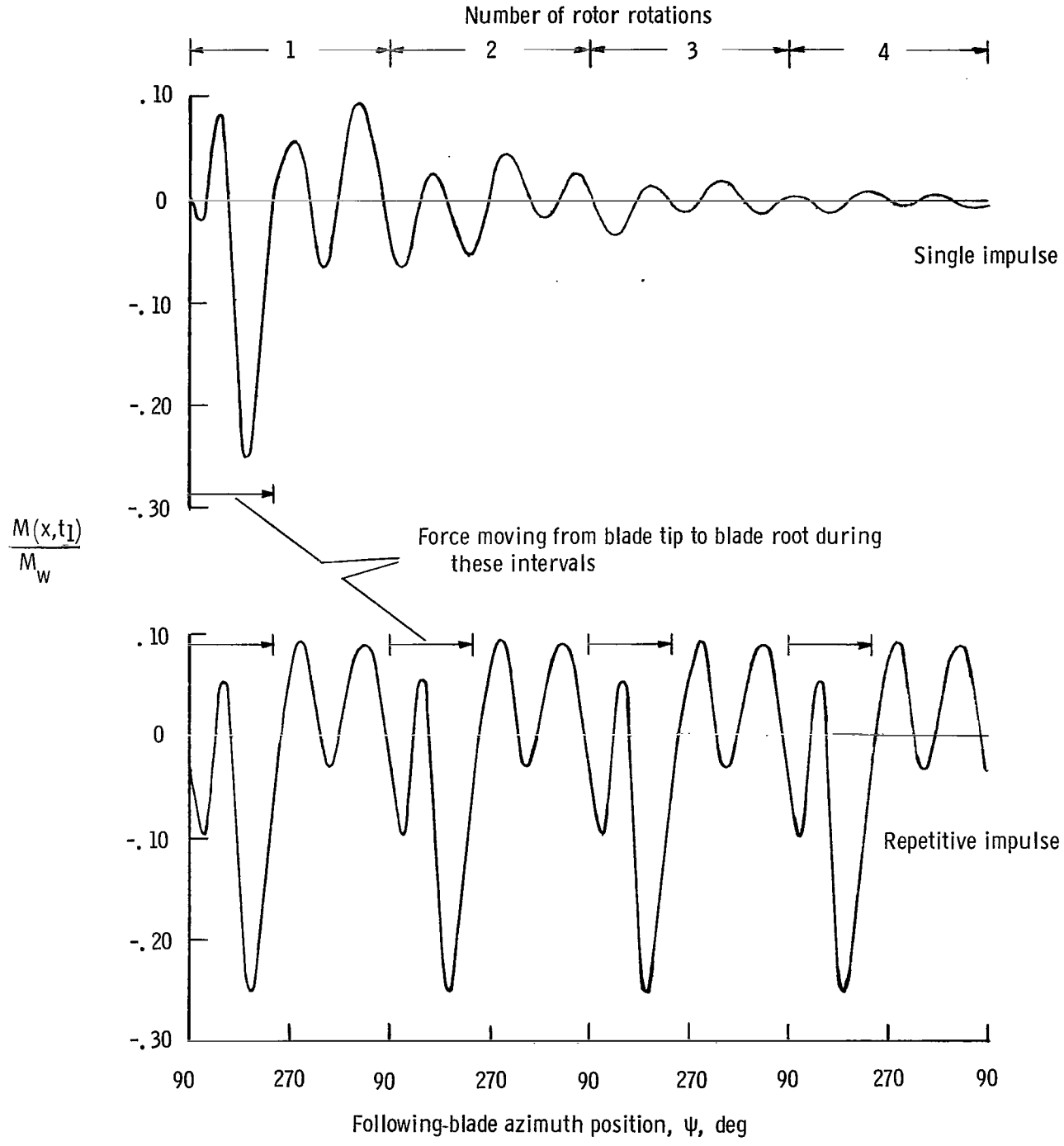

Figure 12.- Blade-root (x = R) flapwise bending moment for single and repetitive impulse. $\varepsilon = 0$; three-blade rotor; $\mu \approx 0.3$ ($\Delta\psi = 150^0$); $n = 3$; $\nu_1 = 0.13$; $\nu_2 = 0.05$; $\nu_3 = 0.07$.

"The aeronautical and space activities of the United States shall be conducted so as to contribute . . . to the expansion of human knowledge of phenomena in the atmosphere and space. The Administration shall provide for the widest practicable and appropriate dissemination of information concerning its activities and the results thereof."

—NATIONAL AERONAUTICS AND SPACE ACT OF 1958

NASA SCIENTIFIC AND TECHNICAL PUBLICATIONS

TECHNICAL REPORTS: Scientific and technical information considered important, complete, and a lasting contribution to existing knowledge.

TECHNICAL NOTES: Information less broad in scope but nevertheless of importance as a contribution to existing knowledge.

TECHNICAL MEMORANDUMS: Information receiving limited distribution because of preliminary data, security classification, or other reasons.

CONTRACTOR REPORTS: Scientific and technical information generated under a NASA contract or grant and considered an important contribution to existing knowledge.

TECHNICAL TRANSLATIONS: Information published in a foreign language considered to merit NASA distribution in English.

SPECIAL PUBLICATIONS: Information derived from or of value to NASA activities. Publications include conference proceedings, monographs, data compilations, handbooks, sourcebooks, and special bibliographies.

TECHNOLOGY UTILIZATION PUBLICATIONS: Information on technology used by NASA that may be of particular interest in commercial and other non-aerospace applications. Publications include Tech Briefs, Technology Utilization Reports and Notes, and Technology Surveys.

Details on the availability of these publications may be obtained from:

SCIENTIFIC AND TECHNICAL INFORMATION DIVISION

NATIONAL AERONAUTICS AND SPACE ADMINISTRATION

Washington, D.C. 20546